Available online at www.sciencedirect.com

SciVerse ScienceDirect

Ceramics International 38 (2012) 3023–3028

CERAMICS INTERNATIONAL

www.elsevier.com/locate/ceramint

Ultra-thin cerium oxide nanostructures through a facile aqueous synthetic strategy

Thadathil S. Sreeremya, Asha Krishnan, Srividhya J. Iyengar, Swapankumar Ghosh *

Nanoceramics Division, National Institute for Interdisciplinary Science and Technology (NIIST), Council of Scientific and Industrial Research (CSIR), Trivandrum 695 019, India

Received 9 November 2011; received in revised form 29 November 2011; accepted 30 November 2011
Available online 8 December 2011

Abstract

In this work, synthesis of ultra-thin 2D CeO_2 nanoribbons is reported for the first time along with rod-shaped nanostructures via a surfactant free aqueous method. CeO_2 nanoribbons of length >100 nm have been synthesised through a mild reaction route involving ammonia precipitation and subsequent heating and ageing at 0 °C. 2D nanostructures are proposed to be formed as a result of self-assembly of CeO_2 molecules. The ribbons exhibited amorphous X-ray diffraction pattern and TEM showed a ribbon like morphology with crystal facets of ~0.33 nm spacing corresponding to (1 1 1) plane of CeO_2. HR-TEM confirmed that the nanorods are enclosed by {1 1 1} planes and have preferentially grown in {1 1 0} direction. The surface area of the powder containing majority nanorods is 82 m^2/g and their average pore size is ~3 nm. The nanostructures exhibited optical band gaps dominated by the regular quantum confinement effect as well as presence of defects.

Keywords: D. CeO_2; Nanoribbon; Nanorods; Ultrathin; Surfactant-free

1. Introduction

The synthesis of anisotropic CeO_2 nanocrystals such as nanorods, nanowires, nanotubes, and nanodisks is of great technological interest because the unique size- and shape-dependent chemical and physical properties show promise in a number of applications ranging from catalysis [1], solid oxide fuel cells (SOFCs) [2], optics [3] to polishing materials [4], gas sensors [5], UV blockers [6] and three-way catalysts (TWCs) [7]. Such materials are also particularly useful in biomedical applications to scavenge the reactive free radicals and oxygen compounds, which are injurious to living cells [8,9]. Nanocrystals with highly anisotropic shapes have larger surface areas, and as a result are metastable [10]. At higher crystal growth rates, in the 'kinetic growth regime', an astonishing variety of highly anisotropic shapes can be obtained [10,11]. The effect of synthetic parameters such as, precursors, concentration, ligands, solvents and reaction temperature on kinetics and thermodynamics has been intensively studied in the fabrication of a variety of CeO_2 nanostructures, including nanorods [7], nanoplates [3,12], hollow spheres [13], nanowires [14] and nanotubes [15]. The synthesis of CeO_2 2D structures deserves special attention for their unusual quantum properties due to the extremely high anisotropy with ultrathin thickness [16] and as they are reported as precursors for the conversion into nanotubes based on the rolling-up mechanism [3]. CeO_2 nanocrystals with rod [7,17] shapes exhibit higher CO conversion at lower temperature [17] and display higher oxygen storage capacity [7] than spheroidal particles, due to the presence of a greater proportion of {1 0 0} and {1 1 0} surfaces. Yu et al. [16] synthesised nanosheets of CeO_2 by the hydrolysis of cerium(III) nitrate with 6-aminohexanoic acid at 95 °C. Ivanov and Polezhaeva reported the synthesis of highly crystalline rhombic CeO_2 nanoplates involving hydrolysis of cerium nitrate in the presence of hexamethylenetetramine [18]. CeO_2 nanorods can be synthesised with 'kinetic shape control' through the introduction of surface (facet) selective molecules [10], by thermal decomposition of cerium oleate complex [19], or by autoclaving cerium nitrate hexahydrate and sodium hydroxide [7,20]. However, synthesis of anisotropic CeO_2 nanostructures e.g., nanorods and ultra-thin 2D structures through surfactant free, low-cost ammonia precipitation

* Corresponding author. Tel.: +91 471 2515385; fax: +91 471 2491712.
E-mail address: swapankumar.ghosh2@mail.dcu.ie (S. Ghosh).

0272-8842/$36.00
doi:10.1016/j.ceramint.2011.11.084

method still remains a great challenge. To the best of our knowledge, there is no other report on the synthesis of CeO_2 nanorods/tubes and ultrathin 2D nanostructures by a surfactant free ammonia precipitation method.

Here, we report for the first time, a simple aqueous chemical method for the synthesis of ribbon like ultrathin CeO_2 nanostructures with mild reaction conditions. Mixed CeO_2 nanorods were produced on increasing the ageing time at 100 °C. The nanostructures were characterised by HR-TEM, X-ray diffraction, BET technique and UV–visible reflectance spectra. All the results are discussed and correlated which shows the possibility of a synthetic strategy in producing ultrathin CeO_2 nanostructures for fabricating fascinating nanostructures which may find use in catalytic, oxygen storage and other industrial applications.

2. Experimental

2.1. Materials

All the syntheses were carried out with double distilled water produced using a quartz glass distillation unit and the chemicals utilised in this study were used as received without further purification. $Ce(NO_3)_3{\cdot}6H_2O$ (99.9%) was purchased from Indian Rare Earths Ltd., India, 25% ammonia solution (analytical grade) was procured from Qualigens Fine Chemicals. Ethyl alcohol (analytical grade) was procured from Merck, India.

2.2. Synthetic methods

An aqueous solution containing 0.042 mol of cerium nitrate was added under vigorous mechanical stirring (using a 1/8 hp overhead stirrer at 2000 rpm) to a 25% ammonia solution at a uniform rate over 1 min. The net cerium ion concentration after complete addition was 0.073 M and the OH:Ce ratio was >10:1 in the reaction mixture. The slurry turned yellow immediately after the addition of ammonia indicating the formation of colloidal CeO_2 particles. The preparation process includes two successive stages of ageing; the first being at 100 °C (for ~15 s and 5 min) followed by the final at 0 °C. The freshly precipitated slurry was divided into two parts. One portion of the aqueous slurry was boiled for ~15 s in a RB flask and removed rapidly from the heating source. The reaction mixture was immediately quenched by dipping the flask in an ice bath maintained at 0 °C and kept for ageing for 30 days. The precipitate was separated by centrifugation and was washed with distilled water and ethanol several times until free from nitrates, and dried at 60 °C overnight in an air-oven. This material will be referred to as Ce-0MIN.

The other part of the slurry was refluxed for 5 min in a RB flask. The hot CeO_2 slurry was then quickly transferred and quenched in an ice bath maintained at 0 °C. The CeO_2 precipitate was aged at 0 °C for 30 days. The colloidal CeO_2 crystals were separated by centrifugation, washed with distilled water and ethanol several times, and finally dried at 60 °C as before. This dried material will be referred to as Ce-5MIN in the remaining text. The sample identification code, their syntheses conditions and selected physical characterisation data are provided in Table 1.

Table 1
Synthesis conditions, their identification code and selected physical properties of different cerium oxide nanostructures.

	Reaction time at 100 °C	
	Ce-0MIN	Ce-5MIN
Particle shape	2D nanoribbon	Nanorod
Crystallite size (nm)	–	11
Particle size (nm)	$L = 100$; $D = 5$	$L = 100$–400; $D = 17$
Lattice parameter (Å)	–	5.435
Bandgap energy (eV)	3.28	3.1

2.3. Characterisation techniques

Crystal structure and size of the powder samples were studied by X-ray diffraction (XRD) analysis. Powder XRD patterns of the as synthesised powder was obtained using Philips X'PERT PRO diffractometer with Ni-filtered Cu $K\alpha_1$ radiation, ($\lambda = 1.5406$ Å) in the 2θ range 20–100 degree at 2° min^{-1} scanning rate and 0.04° step size at 40 mA, 40 kV. The crystallite size (D) of CeO_2 nanocrystals was calculated by using well-known Debye–Scherrer formula [21,22]

$$D = \frac{k\lambda}{\beta \cos\theta} \quad (1)$$

where λ is the wavelength of X-ray, k is the shape factor and has a value of 0.9 in cubic systems, β and θ are the full width at half maximum and the Bragg angle for (1 1 1) reflection, respectively.

The morphology, average size of the CeO_2 nanocrystals and crystal structure were determined by high resolution transmission electron microscopy (HR-TEM) using a FEI Tecnai 30 G^2 S-Twin microscope operated at 300 kV and equipped with a Gatan CCD camera. Samples for TEM study were prepared by dropping a micro droplet of suspension in isopropyl alcohol on to a 400 mesh copper grid and drying the excess solvent naturally. The absorbance and reflectance spectra of the powders were obtained using a UV–visible 2401 PC spectrophotometer (Shimadzu) in the 200–800 nm range which is equipped with an integration sphere for reflectance spectra recording. Nitrogen adsorption–desorption isotherms on CeO_2 samples were recorded at liquid nitrogen temperature (77 K) using a Micromeritics Gemini 2360 surface area analyser. CeO_2 powders were degassed at 200 °C for 5 h in flowing dry nitrogen gas prior to the nitrogen adsorption studies. The surface area of the CeO_2 powders was determined from the Brunauer–Emmett–Teller (BET) equation and analysed with Barrett Joyner Halanda (BJH) method; the pore volumes and pore size distributions were derived from the desorption branches of isotherms.

3. Results and discussion

The HR-TEM images of CeO_2 nanostructures in Ce-0MIN are presented in Fig. 1. Careful inspection of the HR-TEM images of Ce-0MIN reveals the presence of well-defined 2D

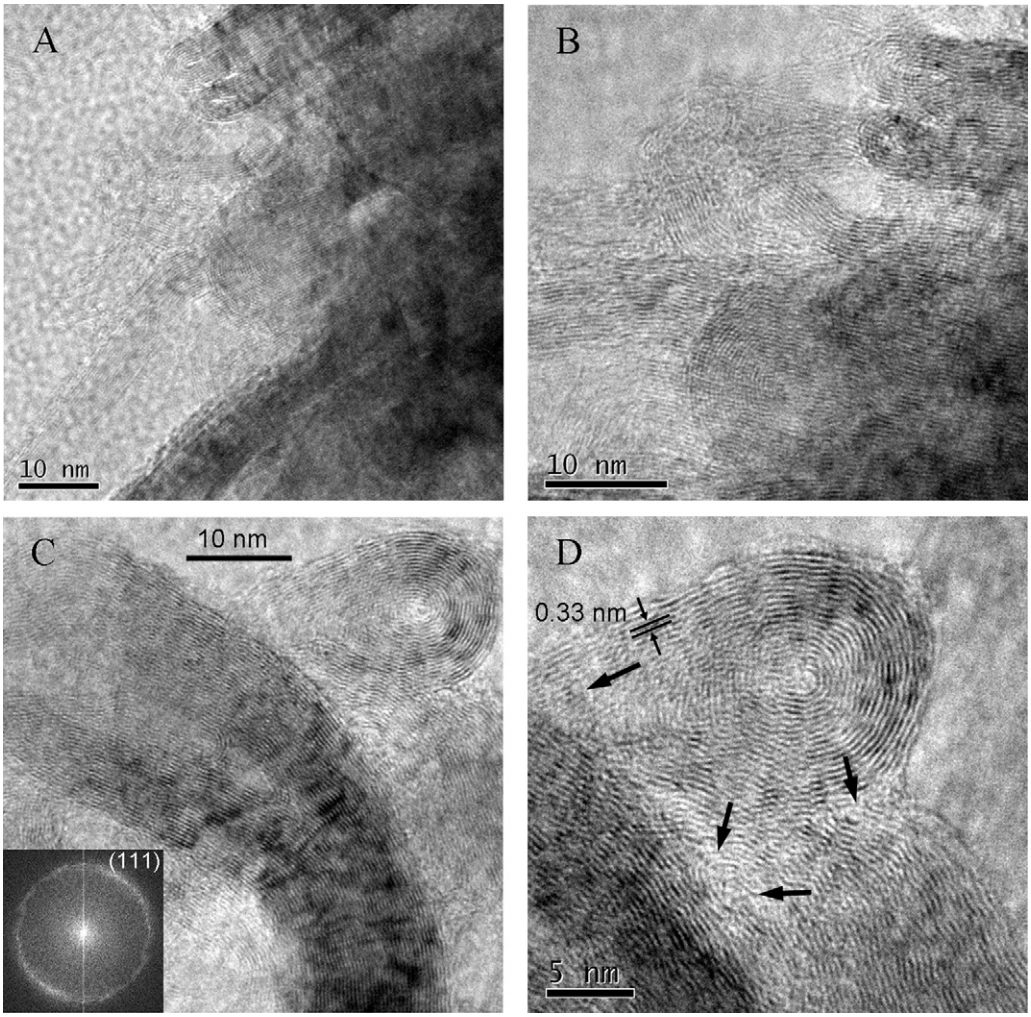

Fig. 1. Characterisation of ceria nanostructures of sample Ce-0MIN. (a and b) TEM image of self-assembly of parallel nanoribbons, (c) TEM images of nanoribbons with the formation of tubular shape at the end with circular head and its first Fourier transform is shown in the inset, and (d) HR-TEM image showing a circular ribbon head with surface defects marked as arrowheads.

CeO_2 nanostructures with ribbon like morphology in as synthesised ceria with exposed (1 1 1) facets of interlayer spacing ~0.33 nm (Fig. 1d) when viewed in the (1 1 1) zone axis. The crystal facets maintained identical spacing throughout the length of the 2D structures. Formation of 2D nanostructures can be explained by the self-assembly of CeO_2 of molecular dimensions, produced during ammonia precipitation. Fig. 1a and 1b indicate the initiation of growth process for the formation of nanotubes with smooth circular heads at one end.

The average diameter of the circular heads at the end of nanoribbons is ~15 nm with length over 100 nm and the ribbons are aligned parallel to each other. The ribbon-like structures are unique and molecular thick, similar to that of graphene [23]. The thickness is confirmed by the presence of only one crystal facet in the X-ray diffraction pattern as well as in fast Fourier transform of HR-TEM images. Such structures were never been reported earlier in CeO_2 system. The fast Fourier transform of the image in Fig. 1c gave only one Debye–Scherrer ring (inset of Fig. 2c) with corresponding interplanar spacing of 0.33 nm, which can be indexed as expanded (1 1 1) reflection of cubic CeO_2 of $Fm\bar{3}m$ space group with evident lattice expansion. The ribbon surfaces are perfectly flat and point defects due to missing atoms or local deformation due to the twist of parallel planes are observed on the surface, marked by arrowheads in Fig. 1d. The ageing at 0 °C for 30 day did not

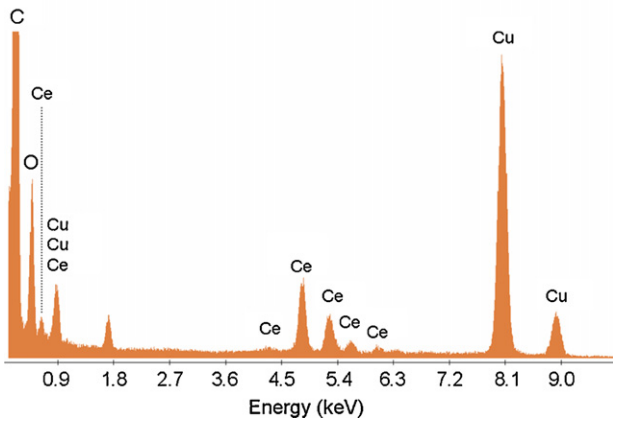

Fig. 2. Energy dispersive spectrum of as synthesised Ce-0MIN powder.

probably allow any fast process involving growth through dissolution–recrystallisation mechanism. A slow build-up process, involving molecules by molecules, fabricated the ultra-thin 2D CeO_2 nanostructures.

The elemental composition of the as-prepared cerium oxide nanoribbons was studied by energy dispersive spectroscopy (EDS) taken during TEM analyses and is shown in Fig. 2. The EDS spectrum shows cerium and oxygen atom in the specimen in a ratio close to 1:2 indicating the presence of CeO_2 in Ce-0MIN. The presence of copper and carbon impurities in the EDS spectrum is contributed by the TEM grid.

The TEM images of Ce-5MIN are shown in Fig. 3. It shows the presence of a mixture of rod- and irregular-shaped particles of CeO_2 in Ce-5MIN. Porous nature of the particle surface is apparent from the TEM images. Slight extension of ageing time from 15 s to 5 min at 100 °C with a high base concentration (OH/Ce ratio > 10) produced predominantly nanorods (Ce-5MIN) from anisotropic growth of unstable $Ce(OH)_3$ nuclei, governed by dissolution–recrystallisation mechanism. Careful inspection of the nanorods reveals the formation of mixed morphology CeO_2 nanorods. Detailed analysis of multiple images reveals that Ce-5MIN contains ~91% nanorods by number with variable length in the range 100–400 nm.

The average diameter of the nanorods from TEM (D_{TEM}) is 15 ± 3 nm. The remaining 9% is highly clustered nanoparticles with an average size $\sim 3.5 \pm 1$ nm. 1D preferential growth is seen in the HR-TEM images of nanorods in {1 1 0} direction with {1 1 1} exposed surface when viewed in the {1 1 1} zone axis. Fast Fourier transform (FFT) analysis of HR image (Fig. 3b) confirms the presence of {1 1 1} and {1 1 0} facets only. By contrast, Yang et al. reported the growth along the [2 1 1] direction [24]. Point defects are observed on nanorod surfaces also (marked by circle in the inset to Fig. 3b). The XRD patterns of as-synthesised ceria powders are shown in Fig. 4. Increase of reaction time from 0 to 5 min at 100 °C transformed 2D ultra-thin CeO_2 to nanorods. The XRD patterns confirm that Ce-5MIN contains relatively more crystalline CeO_2 than in the nanoribbons (Ce-0MIN) which shows the presence of only expanded (1 1 1) crystal plane.

Peaks corresponding to (1 1 1), (2 0 0), (2 2 0) and (3 1 1) planes, with corresponding interplanar spacings of 0.31, 0.27, 0.19, and 0.16 nm respectively, for a fluorite-like cubic CeO_2 were indexed in the XRD pattern of Ce-5MIN (space group: $Fm\bar{3}m$, JCPDS Card No. 34-0394) [21]. The broad XRD peak in Ce-0MIN could be assigned to the (1 1 1) reflection, with a large shift towards higher *d*-values indicating lattice expansion in the synthesised product.

Fig. 5 shows nitrogen adsorption–desorption isotherms and the corresponding distributions of pore sizes in Ce-0MIN and Ce-5MIN ceria powders. The isothermal curves of Ce-5MIN clearly show a small hysteresis in the volume of nitrogen adsorption–desorption over the normal relative pressures range.

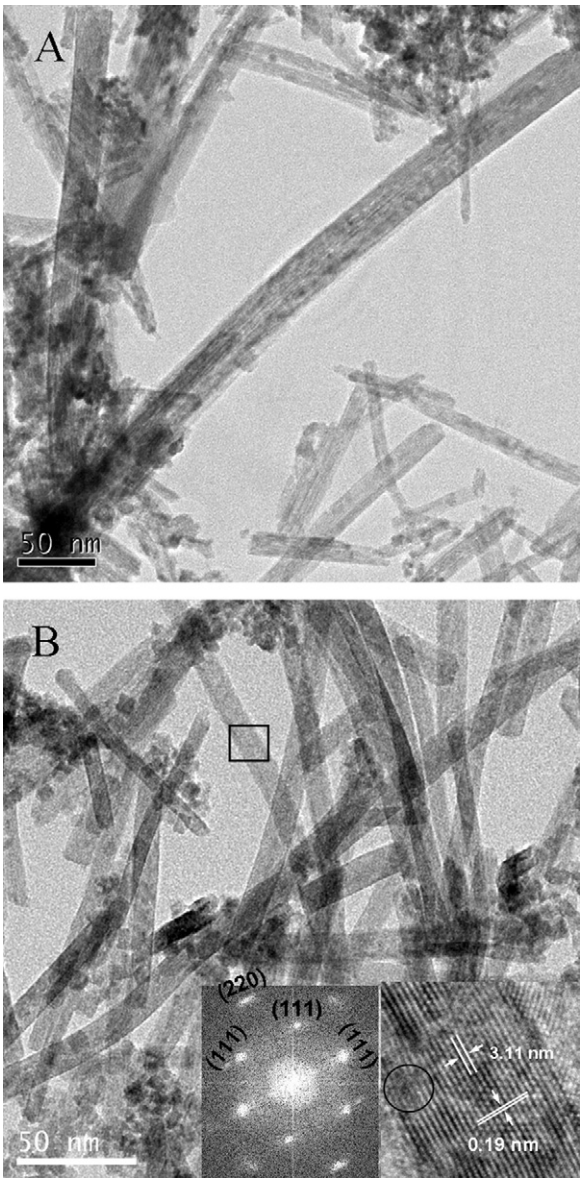

Fig. 3. TEM images of Ce-5MIN samples (a) and (b) with reaction time 5 min at 100 °C, aged at 0 °C for 30 days. The HR-TEM image and fast Fourier transform of the marked region (square) of the nanorod are shown as insets to (b).

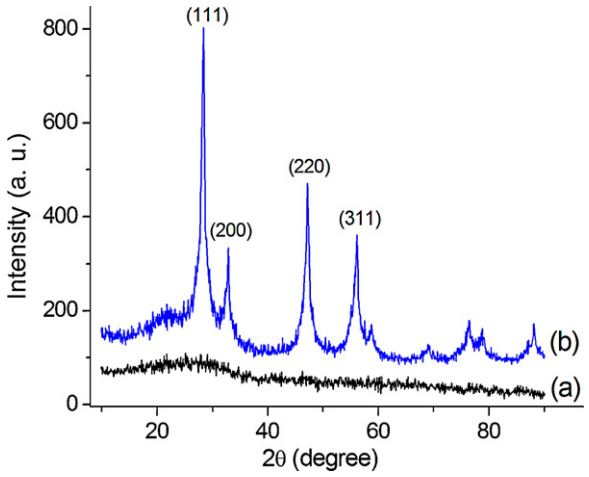

Fig. 4. X-ray diffraction patterns of CeO_2 powders (a) Ce-0MIN, and (b) Ce-5MIN synthesised by ammonia precipitation at 100 °C for different duration of time followed by ageing for 30 days at 0 °C. The XRD pattern of Ce-5MIN is scaled to avoid overlapping.

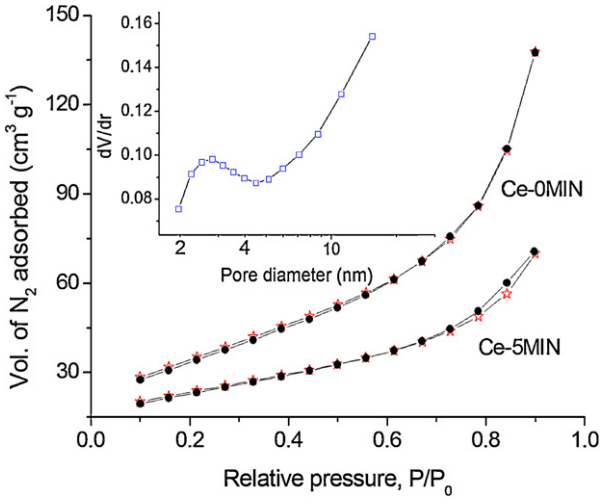

Fig. 5. Nitrogen adsorption–desorption isotherms of Ce-0MIN and Ce-5MIN. The corresponding BJH pore size distribution of Ce-5MIN are shown in the inset.

The BET surface area of Ce-5MIN containing predominantly nanorods is 82 m^2/g. The pore size distribution profile (inset of Fig. 5), is centred at ~3 nm. TEM observation also indicated the presence of surface pores.

Fig. 6 shows the plots of $(\alpha h\nu)^2$ vs. photon energy of CeO_2 nanostructures derived from the reflectance spectra of the powders in the UV–visible range 200–800 nm. The reflectance spectra on the solid specimen extends from 230 nm to 400 nm. The direct band-gap (E_d) is calculated from the onset of the absorption spectrum. E_d obtained for CeO_2 nanoribbons (Ce-0MIN) and Ce-5MIN are 3.28 and 3.1 eV, respectively [25]. Bulk ceria usually absorbs in the UV region with a band gap of 3.2 eV owing to the $O_{2p} \rightarrow Ce_{4f}$ transition and is commonly used as a UV blocker [6]. With respect to bulk ceria, the 2D nanostructures (Ce-0MIN) showed a blue shift in the band gap energy. The variation in band gap from that of bulk ceria is explained by many researchers in terms of quantum confinement effect (blue shift) and also by the presence of defects (red shift) [26,27].

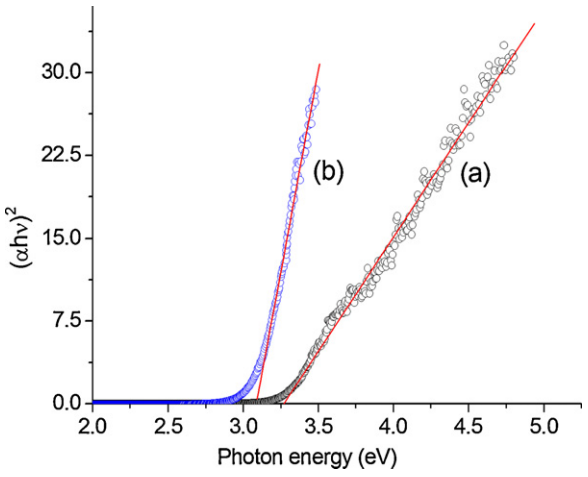

Fig. 6. Plot of $(\alpha h\nu)^2$ vs. photon energy for electronic band-gap measurement of anisotropic CeO_2 nanostructures (a) Ce-0MIN, and (b) Ce-5MIN.

In our case (Ce-0MIN), both the effects are contributing with the predominance of the quantum confinement effect due to the ultrathin thickness of the nanoribbons. CeO_2 nanostructures with majority as rods (Ce-5MIN) have shown marginal red-shift. Simple quantum size effect calculations assume that no significant variation of the chemical structure of the metal oxide is occurring during the particle size reduction [8]. In the case of CeO_2 nanorods, the presence of defects (lead to oxygen vacancies) overcomes the expected influence of the regular quantum size effect, resulting in reduction (red shift) in band-gap energy.

4. Conclusions

In summary, we have reported a facile method to synthesise 2D CeO_2 nanoribbons as well as nanorods from cerium nitrate hexahydrate. Well-defined crystal facets with spacing of ~0.33 nm including the circular array at the end of ribbon shaped crystals were observed in the HR-TEM images and X-ray diffraction pattern of nanoribbons. HR-TEM on nanorods established the presence of surface defects and as a result a marginal red- shift was observed in its optical band gap energy. Rod-shaped CeO_2 nanostructures are enclosed by (1 1 1) facets and shown anisotropic growth in {1 1 0} direction. X-ray diffraction data confirmed the formation of fcc fluorite structured CeO_2 in rod shaped nanocrystals. The formation of the ribbon like CeO_2 nanocrystals from this mild reaction route could prove useful for synthesis of 1D and other 2D nanostructures.

Acknowledgements

This work was financially supported by the Indian Rare Earths Limited Technology Development Council (IRELTDC), DAE, India. We thank Director, NIIST for providing the necessary facilities for the work. We thank Department of Science and Technology and CSIR, India for providing HR-TEM facility to NIIST. Authors acknowledge Mr. M. Kiran for the HR-TEM imaging and analysis. One of the authors (AK) acknowledges CSIR for the CSIR-UGC JRF fellowship.

References

[1] P. Palmisano, N. Russo, P. Fino, D. Fino, C. Badini, High catalytic activity of SCS-synthesized ceria towards diesel soot combustion, Appl. Catal. B 69 (2006) 85–92.
[2] D. Andreescu, E. Matijevic, D.V. Goia, Formation of uniform colloidal ceria in polyol, Colloid Surf. A 291 (2006) 93–100.
[3] C.S. Pan, D.S. Zhang, L.Y. Shi, CTAB assisted hydrothermal synthesis, controlled conversion and CO oxidation properties of CeO_2 nanoplates, nanotubes, and nanorods, J. Solid State Chem. 181 (2008) 1298–1306.
[4] L.Y. Wang, K.L. Zhang, Z.T. Song, S.L. Feng, Ceria concentration effect on chemical mechanical polishing of optical glass, Appl. Surf. Sci. 253 (2007) 4951–4954.
[5] H.I. Chen, H.Y. Chang, Synthesis of nanocrystalline cerium oxide particles by the precipitation method, Ceram. Int. 31 (2005) 795–802.
[6] S. Yabe, T. Sato, Cerium oxide for sunscreen cosmetics, J. Solid State Chem. 171 (2003) 7–11.

[7] H.X. Mai, L.D. Sun, Y.W. Zhang, R. Si, W. Feng, H.P. Zhang, H.C. Liu, C.H. Yan, Shape-selective synthesis and oxygen storage behavior of ceria nanopolyhedra, nanorods, and nanocubes, J. Phys. Chem. B 109 (2005) 24380–24385.
[8] A. Corma, P. Atienzar, H. Garcia, J.Y. Chane-Ching, Hierarchically mesostructured doped CeO_2 with potential for solar-cell use, Nat. Mater. 3 (2004) 394–397.
[9] J.P. Chen, S. Patil, S. Seal, J.F. McGinnis, Rare earth nanoparticles prevent retinal degeneration induced by intracellular peroxides, Nat. Nanotechnol. 1 (2006) 142–150.
[10] Y. Yin, A.P. Alivisatos, Colloidal nanocrystal synthesis and the organic–inorganic interface, Nature 437 (2005) 664–670.
[11] Y.C. Cao, Synthesis of square gadolinium-oxide nanoplates, J. Am. Chem. Soc. 126 (2004) 7456–7457.
[12] H.L. Lin, C.Y. Wu, R.K. Chiang, Facile synthesis of CeO_2 nanoplates and nanorods by [1 0 0] oriented growth, J. Colloid Interface Sci. 341 (2010) 12–17.
[13] Y.T. Song, J.J. Wei, Y.Z. Yang, Z.J. Yang, H.X. Yang, Preparation of CeO_2 hollow spheres via a surfactant-assisted solvothermal route, J. Mater. Sci. 45 (2010) 4158–4162.
[14] B. Tang, L.H. Zhuo, J.C. Ge, G.L. Wang, Z.Q. Shi, J.Y. Niu, A surfactant-free route to single-crystalline CeO_2 nanowires, Chem. Commun. (2005) 3565–3567.
[15] W.Q. Han, L.J. Wu, Y.M. Zhu, Formation and oxidation state of CeO_{2-x} nanotubes, J. Am. Chem. Soc. 127 (2005) 12814–12815.
[16] T. Yu, B. Lim, Y.N. Xia, Aqueous-phase synthesis of single-crystal ceria nanosheets, Angew. Chem. Int. Ed. 49 (2010) 4484–4487.
[17] K.B. Zhou, X. Wang, X.M. Sun, Q. Peng, Y.D. Li, Enhanced catalytic activity of ceria nanorods from well-defined reactive crystal planes, J. Catal. 229 (2005) 206–212.
[18] V.K. Ivanov, O.S. Polezhaeva, Synthesis of ultrathin ceria nanoplates, Russ. J. Inorg. Chem. 54 (2009) 1528–1530.
[19] A. Ahniyaz, Y. Sakamoto, L. Bergstrom, Tuning the aspect ratio of ceria nanorods and nanodumbbells by a face-specific growth and dissolution process, Cryst. Growth Des. 8 (2008) 1798–1800.
[20] Z.Q. Yang, K.B. Zhou, X.W. Liu, Q. Tian, D.Y. Lu, S. Yang, Single-crystalline ceria nanocubes: size-controlled synthesis, characterization and redox property, Nanotechnology 18 (2007) 185606 (4pp.).
[21] S. Ghosh, D. Divya, K.C. Remani, T.S. Sreeremya, Growth of monodisperse nanocrystals of cerium oxide during synthesis and annealing, J. Nanopart. Res. 12 (2010) 1905–1911.
[22] M. Chakraborty, S. Dasgupta, S. Sengupta, J. Chakraborty, S. Ghosh, J. Ghosh, M. Mitra, A. Misra, T.K. Mandal, D. Basu, A facile synthetic strategy for Mg–Al layered double hydroxide material as nanocarrier for methotrexate, Ceram. Int. 38 (2012) 941–949.
[23] S. Chen, J.W. Zhu, X. Wang, An in situ oxidation route to fabricate graphene nanoplate–metal oxide composites, J. Solid State Chem. 184 (2011) 1393–1399.
[24] N. Du, H. Zhang, B.G. Chen, X.Y. Ma, D.R. Yang, Ligand-free self-assembly of ceria nanocrystals into nanorods by oriented attachment at low temperature, J. Phys. Chem. C 111 (2007) 12677–12680.
[25] H.P. Zhou, Y.W. Zhang, H.X. Mai, X. Sun, Q. Liu, W.G. Song, C.H. Yan, Spontaneous organization of uniform CeO_2 nanoflowers by 3D oriented attachment in hot surfactant solutions monitored with an in situ electrical conductance technique, Chem. Eur. J. 14 (2008) 3380–3390.
[26] S. Maensiri, C. Masingboon, P. Laokul, W. Jareonboon, V. Promarak, P.L. Anderson, S. Seraphin, Egg white synthesis and photoluminescence of plate-like clusters of CeO_2 nanoparticles, Cryst. Growth Des. 7 (2007) 950–955.
[27] T.S. Sreeremya, K.M. Thulasi, A. Krishnan, S. Ghosh, A Novel Aqueous Route to Fabricate Ultrasmall Monodisperse Lipophilic Cerium Oxide Nanoparticles, Ind. Eng. Chem. Res. 51 (2012) 318–326.